

Salivary gland tumors of the parotid gland: CT and MR imaging findings with emphasis on intratumoral cystic components

Hiroki Kato · Masayuki Kanematsu · Haruo Watanabe ·
Keisuke Mizuta · Mitsuhiro Aoki

Received: 11 December 2013 / Accepted: 1 May 2014 / Published online: 20 June 2014
© Springer-Verlag Berlin Heidelberg 2014

Abstract

Introduction The purpose of this study was to assess computed tomography (CT) and magnetic resonance (MR) imaging findings of salivary gland tumors of the parotid gland with emphasis on intratumoral cystic components.

Methods Seventy-two histopathologically confirmed salivary gland tumors of the parotid gland (44 benign and 28 malignant), which underwent both CT and MR imaging including contrast-enhanced study, were included in this study. We retrospectively reviewed images for the presence, number, occupying rate, margin characteristics, distribution, and predominant MR signal intensity of intratumoral cystic components.

Results The prevalence of cystic components was greater in malignant than benign tumors (79 vs. 50 %, $p<0.05$). The number and occupying rate were similar between benign and malignant tumors. The irregular margins were more frequent in malignant than benign tumors (73 vs. 27 %, $p<0.01$). The frequency of eccentric location was greater in benign than malignant tumors (91 vs. 55 %, $p<0.01$), whereas the frequency of centric location was greater in malignant than benign tumors (32 vs. 0 %, $p<0.01$). On T1-weighted images, the frequency of hyperintensity was greater in benign than malignant tumors (50 vs. 9 %, $p<0.01$), whereas that of isointensity

was greater in malignant than benign tumors (50 vs. 0 %, $p<0.01$). Multiple logistic regression analysis showed that the absence of irregular margins of cystic components only was significantly correlated with the presence of benign salivary gland tumors ($p<0.01$).

Conclusion Imaging features of intratumoral cystic components may help to differentiate benign from malignant tumors of the parotid salivary gland.

Keywords Parotid gland · Salivary gland tumor · Cystic component · CT · MRI

Introduction

Computed tomography (CT) and magnetic resonance (MR) imaging findings for the differentiation of benign and malignant salivary gland tumors have been well described, primarily emphasizing on MR signal intensities [1–3], margins [2,3], growth patterns [1–3], dynamic contrast enhancement patterns [4,5], and apparent diffusion coefficients of diffusion-weighted MR imaging [6,7]. Meanwhile, cystic degeneration and tumor necrosis have been reported as common imaging features of salivary gland tumors including pleomorphic adenomas [8], Warthin tumors [9,10], basal cell adenomas [11–13], mucoepidermoid carcinomas [14], adenoid cystic carcinomas [14], acinic cell carcinomas [15], and salivary duct carcinomas [16].

Both cystic degeneration and tumor necrosis were shown as similar unenhanced areas on contrast-enhanced CT and MR imaging. However, the configuration and location of cystic components is bound to be different between cystic degeneration and tumor necrosis due to the difference of mechanism of cyst formation. In addition, because cystic components contain various kinds of fluid material, CT attenuation or MR signal intensity may be able to demonstrate the difference of fluid material.

H. Kato · M. Kanematsu (✉) · H. Watanabe
Department of Radiology, Gifu University School of Medicine,
1-1 Yanagido, Gifu 501-1194, Japan
e-mail: masa_gif@yahoo.co.jp

M. Kanematsu
High-Level Imaging Diagnosis Center, Gifu University Hospital,
Gifu, Japan

K. Mizuta · M. Aoki
Department of Otolaryngology, Gifu University School of Medicine,
Gifu, Japan

However, our literature search did not find any reports on CT and MR imaging findings focused on intratumoral cystic components to differentiate benign from malignant salivary gland tumors. Therefore, the purpose of this study was to evaluate CT and MR imaging findings of salivary gland tumors of the parotid gland emphasizing on intratumoral cystic components.

Methods

Patients

The study was approved by the human research committee of the institutional review board and complied with the guidelines of the Health Insurance Portability and Accountability Act. The requirement for informed consent was waived due to the retrospective nature of this study. We searched the electronic medical chart system of Gifu University Hospital for patients with histopathologically confirmed salivary gland tumors of the parotid gland between July 2004 and August 2013 and identified 163 consecutive patients. Of these, 72 patients (46 men and 26 women, mean age 63 years, age range 17–87 years) which underwent both CT and MR imaging including contrast-enhanced study before histopathological examination were included in the present study. Ninety one patients were excluded, because they did not undergo contrast-enhanced imaging or underwent either CT or MR imaging.

Histopathological evaluation was performed on the basis of findings in specimens obtained at biopsy or surgical resection. Although five patients with Warthin tumors had multifocal or bilateral tumors, the maximum tumor per patient was assessed. The histopathological diagnoses of 72 salivary gland tumors included 44 benign tumors (20 pleomorphic adenomas, 20 Warthin tumors, 3 basal cell adenomas, and 1 oncocytoma) and 28 malignant tumors [7 salivary duct carcinomas, 5 mucoepidermoid carcinomas, 4 epithelial myoepithelial carcinomas, 4 acinic cell carcinomas, 3 carcinoma ex pleomorphic adenomas, 3 adenocarcinomas not otherwise specified (NOS), 1 adenoid cystic carcinoma, and 1 small cell carcinoma].

CT imaging

An eight-slice CT (LightSpeed Ultra, GE Healthcare, Milwaukee, WI, USA) was used. Unenhanced CT images were obtained in all 72 salivary gland tumors (44 benign and 28 malignant), and contrast-enhanced CT images were obtained in 59 salivary gland tumors (38 benign and 21 malignant). Transverse CT images were reconstructed at a section thickness of 2.5 mm with no overlap. Contrast-enhanced two-phase CT imaging was started 45 and 120 s after initiating an intravenous bolus injection of 100 ml of nonionic iodine

contrast material [Optiray 240 (240 mg of iodine/ml); Mallinckrodt, Hazelwood, MO, USA] at an injection rate of 2 ml/s.

MR imaging

A 1.5-T MR imaging system (Intera Achieva 1.5 T Pulsar, Philips Medical Systems, Netherlands) was used. Unenhanced MR images were obtained in all 72 salivary gland tumors (44 benign and 28 malignant), and gadolinium-enhanced MR images were obtained in 56 salivary gland tumors (25 benign and 21 malignant). Transverse MR images were obtained using the parallel imaging technique at 4-mm section thickness with 1-mm intersection gap. Non-fat suppressed T1-weighted spin-echo (TR/TE 630–827/9–15 ms, imaging matrices 512×512, field of view 20×20 cm, parallel imaging factor 1.5) and non-fat suppressed T2-weighted fast spin-echo (TR/TE 4,102–5,710/90 ms, imaging matrices 512×512, field of view 20×20 cm, parallel imaging factor 1.5) images were obtained. Gadolinium-enhanced fat-suppressed T1-weighted spin-echo images (TR/TE 630–840/9–15 ms, imaging matrices 512×512, field of view 20×20 cm, parallel imaging factor 1.5) were obtained after the intravenous injection of 0.1 mmol/kg of gadopentetate dimeglumine (Magnevist; Bayer Healthcare, Berlin, Germany).

Image assessment

Two radiologists with 14 and 8 years of post-training experience of head and neck imaging independently reviewed images, and any disagreements were resolved in consensus. The observer was unaware of patient names, laboratory results, other imaging findings, or final diagnoses. The observer evaluated the presence, number, occupying rate, margin characteristics, distribution, predominant CT attenuation, and predominant MR signal intensity of intratumoral cystic components within salivary gland tumors. The presence of intratumoral cystic components was assessed using contrast-enhanced CT or MR images, and cystic components, including cystic degeneration and necrosis, were defined as unenhanced areas. The occupying rate of cystic components was qualitatively graded using a four-point scale: 1 small occupying areas of 1–25 % of the tumor, 2 moderate (26–50 %), 3 extensive (51–75 %), and 4 diffuse (76–100 %). The characteristics of cystic component margins were assessed for the presence of irregularities. Intratumoral cystic components were classified into three locations: eccentric, central, and entire. Predominant CT attenuations and MR signal intensities of the cystic components were assessed in comparison with those of cerebral gray matter. The maximum diameter of salivary gland tumors and intratumoral cystic components were also measured.

Statistical analysis

Statistical analysis was performed using SPSS version 18.0 statistical software (SPSS, an IBM Company, Chicago, IL, USA). A two-sample *t* test for independent samples with equal variances was used to compare the maximum diameters of tumors and the maximum diameter, numbers, and occupying rates of cystic components between benign and malignant tumors. The Chi-square or Fisher's exact test was also performed to compare the presence, margin characteristics, distributions, unenhanced CT attenuations, and MR signal intensities between benign and malignant tumors. The maximum diameter, numbers, occupying rates, margin characteristics, distributions, unenhanced CT attenuations, and signal intensities on T1- and T2-weighted images of cystic components were used as the variables for multiple logistic regression analysis, and the outcome was benign or malignant. The Hosmer–Lemeshow test was used to assess the goodness of fit of the logistic regression model [17]. Interobserver variability was assessed using kappa statistics. Null hypotheses of no difference were rejected if *p* values were less than 0.05.

Results

Qualitative findings and quantitative measurements are summarized in Table 1. The mean maximum diameter of malignant tumors was significantly greater than that of benign tumors (33.7 ± 14.3 vs. 26.6 ± 10.1 mm, $t(70)=2.45$, $p<0.05$). Intratumoral cystic components were found in 44 tumors (22 benign, 22 malignant) and were significantly more frequent in malignant than benign tumors [$22/28$ (79 %) vs. $22/44$ (50 %),

Table 1 Qualitative imaging findings and quantitative measurements with salivary gland tumors of the parotid gland

	Benign	Malignant
Qualitative imaging findings		
Presence of cystic components [†]	22/44 (50)	22/28 (79)
Irregular margin of cystic components ^{††}	6/22 (27)	16/22 (73)
Quantitative measurements		
Maximum diameter of parotid tumors [†]	26.6±10.1	33.7±14.3
Maximum diameter of cystic components ^{††}	17.1±12.5	16.1±9.8
Number of cystic components ^{††}	2.1±1.8	3.2±4.0
Occupying rate of cystic components ^{††}	2.1±1.2	2.1±1.2

In qualitative imaging findings, data are numbers of tumors, and numbers in *parentheses* are frequencies expressed as percentages. In quantitative measurements, data are shown with the mean±1 standard deviation

[†] The frequency or value was compared between benign ($n=44$) and malignant ($n=28$) tumors

^{††} The frequency or value was compared between benign ($n=22$) and malignant ($n=22$) tumors accompanied by intratumoral cystic components

$p<0.05$; Figs. 1–2]. Irregular margins of cystic components were significantly more frequent in malignant than benign tumors [$16/22$ (73 %) vs. $6/22$ (27 %), $p<0.01$; Figs. 1–2]. The mean maximum diameter [17.1 ± 12.5 and 16.1 ± 9.8 mm, $t(42)=0.30$, $p=0.77$], number [2.1 ± 1.8 and 3.2 ± 4.0 , $t(42)=1.16$, $p=0.25$], and occupying rate [2.1 ± 1.2 and 2.1 ± 1.2 , $t(42)=0.13$, $p=0.90$] of cystic components were not significantly different between benign and malignant tumors, respectively. The frequencies of cystic components in each parotid tumor are also shown in Table 2.

In 44 tumors with cystic components (22 benign, 22 malignant), intratumoral cystic components were eccentrically located in $20/22$ (91 %) and $12/22$ (55 %), centrally in $0/22$ (0 %) and $7/22$ (32 %), and entirely in $2/22$ (9 %) and $3/22$ (14 %) of the benign and malignant tumors, respectively (Table 3). Intratumoral cystic components were eccentrically located significantly more frequently in benign than malignant tumors ($p<0.01$), whereas a centric location was significantly more frequent in malignant than benign tumors ($p<0.01$).

On T1-weighted images, intratumoral cystic components appeared as hyperintense in $11/22$ (50 %) and $2/22$ (9 %), isointense in $0/22$ (0 %) and $11/22$ (50 %), and hypointense in $11/22$ (50 %) and $9/22$ (41 %) of the benign and malignant tumors, respectively (Table 3). On T1-weighted images, hyperintensity of cystic components was significantly more frequent in benign than malignant tumors ($p<0.01$), whereas isointensity was significantly more frequent in malignant than benign tumors ($p<0.01$). There were 11 benign tumors that showed T1 hyperintensity of cystic components, and the Warthin tumors occupied $9/11$ (82 %) of benign tumors with T1 hyperintensity (Table 2; Fig. 1c). T1 hyperintensity of cystic components was observed in $9/12$ (82 %) of Warthin tumors and in $2/2$ (100 %) of basal cell adenomas (Table 2).

T2 signal intensity and unenhanced CT attenuation of intratumoral cystic components were not significantly different between the benign and malignant tumors (Table 3).

Multiple logistic regression analysis showed that the absence of irregular margins of cystic components (odds ratio 7.11, $p=0.004$) only was significantly correlated with the presence of benign salivary gland tumors. The Hosmer–Lemeshow goodness-of-fit χ^2 value was 8.07 ($p=0.43$).

The kappa values for the two observers with regard to evaluating the occupying rates, margin characteristics, distributions, unenhanced CT attenuations, and signal intensities on T1- and T2-weighted images of cystic components showed substantial agreement (mean 0.71, range 0.56–0.85).

Discussion

In pleomorphic adenomas, focal or partial cystic degeneration, tiny hemorrhagic foci, and small infarcted areas are occasionally observed on pathological examinations, but extensive

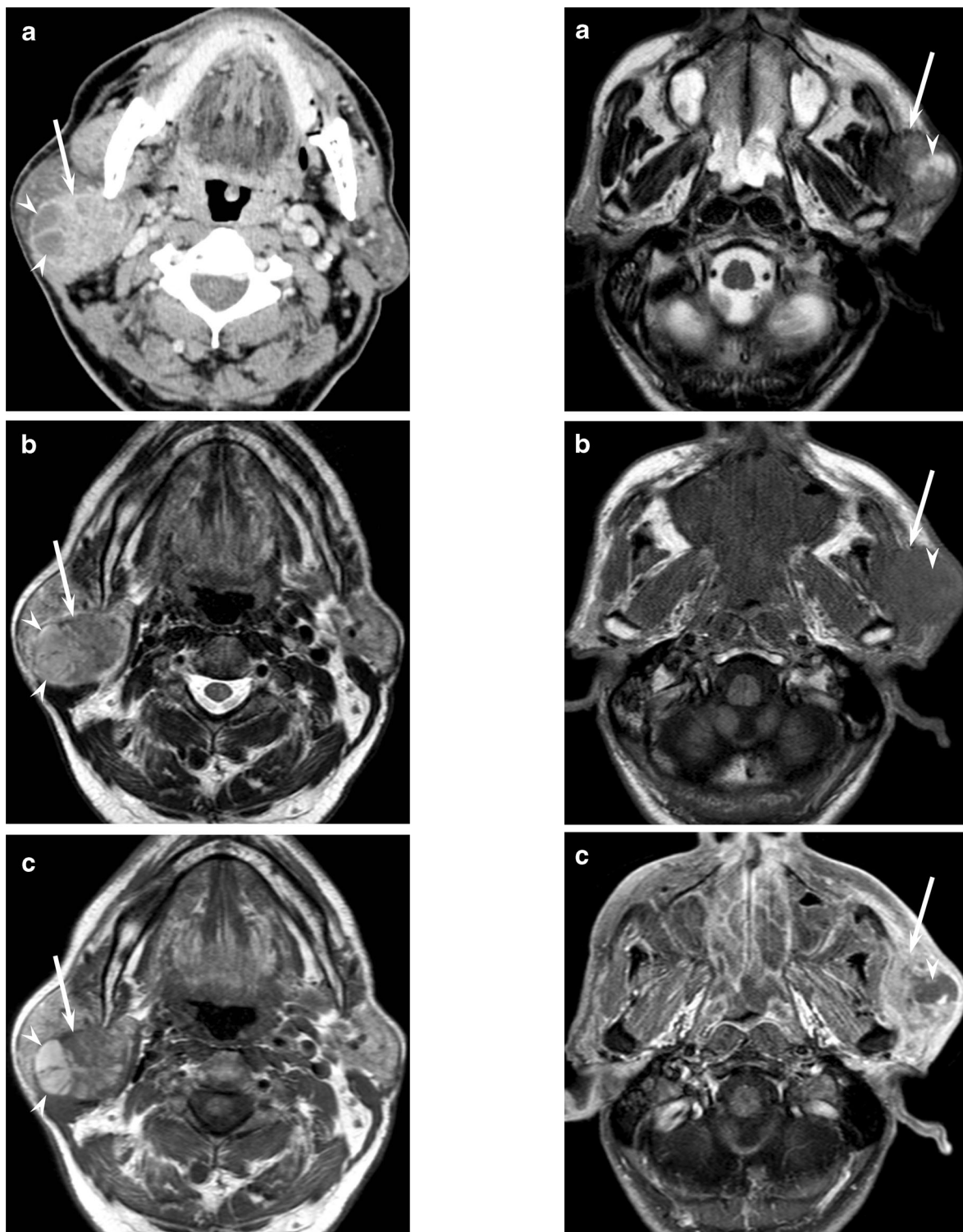


Fig. 1 A 68-year-old man with Warthin tumor of the right parotid gland. **a** Contrast-enhanced CT shows a well-circumscribed lesion in the right parotid gland (*arrow*). Intratumoral cystic components eccentrically appear as hypodense without irregular margins (*arrow heads*). **b** T2-weighted fast spin-echo MR image (TR/TE, 5,710/90 ms) shows a isointense lesion (*arrow*) accompanied by slightly hyperintense cystic components (*arrow heads*). **c** T1-weighted spin-echo images (TR/TE, 779/15 ms) shows a hypointense lesion (*arrows*) accompanied by intensely hyperintense cystic components (*arrow heads*)

cystic degeneration is rare [18]. Although the mechanism of extensive cystic degeneration of pleomorphic adenomas is unclear, several mechanisms may be responsible for causing fine-needle aspiration-associated tumor necrosis [19]. Extensive squamous metaplasia, containing mucinous material, and intratumoral hemorrhage also cause large cyst formations within pleomorphic adenomas [20]. In this study, cystic

Fig. 2 A 69-year-old man with high-grade mucoepidermoid carcinoma of the left parotid gland. **a** T2-weighted fast spin-echo MR image (TR/TE, 4,102/90 ms) shows a ill-circumscribed lesion in the left parotid gland (*arrow*). Intratumoral cystic component eccentrically appears as hyperintense with irregular margins (*arrow head*). **b** T1-weighted spin-echo images (TR/TE, 630/9 ms) shows a hypointense lesion (*arrows*). Intratumoral cystic component cannot be detected due to their isointensity (*arrow head*). **c** Gadolinium-enhanced fat-suppressed T1-weighted spin-echo images (TR/TE, 630/9 ms) clearly shows a irregular cystic component (*arrow head*) within an infiltrative lesion (*arrow*)

components of pleomorphic adenomas almost always showed hypointensity on T1-weighted images and hyperintensity on T2-weighted images.

Most Warthin tumors vary from partly to predominantly cystic, and cystic formation has been reported in approximately 30 % cases [9]. Various numbers of cystic components filled with mucoid or brown fluid in Warthin tumors vary in size from small slit-like spaces to several centimeters in length and occupy a considerable portion of the entire lesion. Focal hyperintense areas of Warthin tumors on T1-weighted images correspond to areas with accumulations of microscopic cysts, containing proteinous fluid with foamy cells, red cells, and neutrophils [10]. Some hyperintense areas on T1-weighted images show characteristic hypointensity on short tau inversion recovery (STIR) images [10]. In this study, approximately half of Warthin tumors were accompanied by cystic components, which generally appeared as hyperintense on T1-weighted images, as previously reported.

Histopathologically, cystic formation of basal cell adenomas is frequently observed, that is produced by cystic dilatation of microglands in the cell clusters or by a unique stromal

Table 3 Imaging findings of cystic components

	Benign (n=22)	Malignant (n=22)
Distribution		
Eccentric	20 (91)*	12 (55)
Central	0 (0)	7 (32)**
Entire	2 (9)	3 (14)
Signal intensity on T1-weighted images		
Hyperintense	11 (50)*	2 (9)
Isointense	0 (0)	11 (50)**
Hypointense	11 (50)	9 (41)
Signal intensity on T2-weighted images		
Hyperintensity	14 (64)	16 (73)
Isointensity	2 (9)	1 (5)
Hypointensity	6 (27)	5 (23)
Unenhanced CT attenuation		
Hyperdensity	3 (14)	2 (9)
Isodensity	4 (18)	9 (41)
Hypodensity	15 (68)	11 (50)

Data are numbers of tumors, and numbers in parentheses are frequencies expressed as percentages

* The frequency of benign tumors was significantly greater than that of malignant tumors ($p < 0.01$)

** The frequency of malignant tumors was significantly greater than that of benign tumors ($p < 0.01$)

alteration such as dilatation of lymphatic vessels [21]. On CT or MR imaging, approximately half of basal cell adenomas are accompanied by cystic components [12,13]. Cystic changes

Table 2 Frequency and MR signal intensity of cystic components in each Parotid Tumor

Histopathologic diagnoses	Presence of cystic components	T1-WI			T2-WI		
		Hyper	Iso	Hypo	Hyper	Iso	Hypo
<i>Benign</i>							
Pleomorphic adenoma	8/20 (40)	0	0	8	7	0	1
Warthin tumor	12/20 (60)	9	0	3	5	2	5
Basal cell adenoma	2/3 (67)	2	0	0	2	0	0
Oncocytoma	0/1 (0)						
<i>Malignant</i>							
Salivary duct carcinoma	6/7 (86)	1	3	2	2	1	3
Mucoepidermoid carcinoma	4/5 (80)	0	3	1	4	0	0
Epithelial myoepithelial carcinoma	3/4 (75)	0	1	2	2	0	1
Acinic cell carcinoma	2/4 (50)	0	0	2	2	0	0
Carcinoma ex pleomorphic adenoma	3/3 (100)	0	3	0	3	0	0
Adenocarcinoma NOS	3/3 (100)	1	1	1	2	0	1
Adenoid cystic carcinoma	1/1 (100)	0	0	1	1	0	0
Small cell carcinoma	0/1 (0)						

In the row of presence of cystic components, data are numbers of tumors, and numbers in parentheses are frequencies expressed as percentages. In the rows of T1- and T2-WI, data are numbers of tumors which underwent MR imaging

mostly occur in tumors at the deeper parts of the superficial lobe or in the deep lobe [13]. Basal cell adenomas in the present study tended to contain hyperintense cystic components on T1-weighted images, because the cystic lumens were generally filled with mucinous materials.

Pathologically, low-grade mucoepidermoid carcinomas contain abundant mucous cells accompanied by their products, resulting in a cystic architectural pattern. Therefore, low-grade mucoepidermoid carcinomas are characterized by cysts containing mucinous materials that appear as hyperintense spots within the tumors on both T1- and T2-weighted images [14]. Large low-grade adenoid cystic carcinomas have been reported to contain hyperintense areas on T1-weighted images, corresponding to hemorrhagic necrosis [14]. Acinic cell carcinoma is one type of low-grade malignant salivary gland tumor, and hyperintense portions on T1- and T2-weighted images can be observed, reflecting hemorrhage on microscopic examination [15]. Despite these previous reports, hyperintense areas on T1-weighted images were not observed in low-grade malignant salivary gland neoplasms in this study.

In high-grade malignant salivary gland neoplasms, including salivary duct carcinomas, high-grade mucoepidermoid carcinomas, high-grade adenoid cystic carcinomas, and high-grade adenocarcinomas NOS, hemorrhage and necrosis are generally observed on gross specimen. Therefore, cystic components can show various signal intensities dependent on the time after hemorrhage and the degree of concentration of necrotic tissue. In this study, although high-grade malignancies tended to contain isointense cystic components on T1-weighted images, one salivary duct carcinoma and one high-grade adenocarcinoma NOS contained hyperintense cystic components on T1-weighted images.

According to these references, cystic components of benign tumors usually result from cystic degeneration, whereas those of malignant tumors usually result from necrosis or hemorrhage. Therefore, we assumed that malignant tumor tended to show irregular margin of cystic components due to necrosis or hemorrhage. Meanwhile, prolonged deprivation of oxygen will lead to chronic hypoxic stress, leading to tumor necrosis. Tumor hypoxia appears to be strongly associated with tumor propagation and malignant progression, and malignant tumors frequently outgrow their oxygen supply. Because hypoxic areas usually occur in the center of tumors, we assumed that centric location of cystic components was more frequent in malignant tumors.

However, because the imaging findings of cystic component in parotid salivary gland tumors were widely overlapping between benign and malignant tumors, it is difficult to use these findings with great confidence. Particularly in benign tumors, the imaging findings showed widely divergent results of MR signal intensity between Warthin tumors and pleomorphic adenomas.

The present study has several limitations. First, the study sample was small, because this study was conducted at a single institution. Second, although we did not perform both contrast-enhanced CT and MR imaging in all patients, we could assess the presence of cystic components on contrast-enhanced CT or MR imaging. Third, we assessed only transverse images, but coronal or sagittal images are also necessary for evaluating the distribution and configuration of cystic components.

In summary, intratumoral cystic component formation and irregular margins of cystic components were more frequently observed in malignant than benign tumors. Intratumoral cystic components tended to eccentrically occur in benign tumors and centrally in malignant tumors. On T1-weighted images, hyperintensity of cystic components were more frequently observed in benign than in malignant tumors. The absence of irregular margins was most reliable findings of cystic components for the diagnosis of benign salivary gland tumor. These imaging features may incrementally add useful information to the differentiation of parotid salivary gland tumors.

Ethical standards and patient consent We declare that all human and animal studies have been approved by the local ethics committee and have therefore been performed in accordance with the ethical standards laid down in the 1964 Declaration of Helsinki and its later amendments. We declare that all patients gave informed consent prior to inclusion in this study.

Conflict of interest We declare that we have no conflict of interest.

References

1. Joe VQ, Westesson PL (1994) Tumors of the parotid gland: MR imaging characteristics of various histologic types. *Am J Roentgenol* 163(2):433–438
2. Takashima S, Wang J, Takayama F, Momose M, Matsushita T, Kawakami S, Saito A, Ishiyama T (2001) Parotid masses: prediction of malignancy using magnetization transfer and MR imaging findings. *Am J Roentgenol* 176(6):1577–1584
3. Christe A, Waldherr C, Hallett R, Zbaeren P, Thoeny H (2011) MR imaging of parotid tumors: typical lesion characteristics in mr imaging improve discrimination between benign and malignant disease. *Am J Neuroradiol* 32(7):1202–1207. doi:10.3174/Ajnr.A2520
4. Choi DS, Na DG, Byun HS, Ko YH, Kim CK, Cho JM, Lee HK (2000) Salivary gland tumors: evaluation with two-phase helical CT. *Radiology* 214(1):231–236. doi:10.1148/radiology.214.1.r00ja05231
5. Yabuuchi H, Fukuya T, Tajima T, Hachitanda Y, Tomita K, Koga M (2003) Salivary gland tumors: diagnostic value of gadolinium-enhanced dynamic MR imaging with histopathologic correlation. *Radiology* 226(2):345–354. doi:10.1148/radiol.2262011486
6. Matsushima N, Maeda M, Takamura M, Takeda K (2007) Apparent diffusion coefficients of benign and malignant salivary gland tumors. Comparison to histopathological findings. *J Neuroradiol* 34(3):183–189. doi:10.1016/j.neurad.2007.04.002
7. Habermann CR, Arndt C, Graessner J, Diestel L, Petersen KU, Reitmeier F, Ussmuller JO, Adam G, Jaehne M (2009) Diffusion-

- weighted echo-planar MR imaging of primary parotid gland tumors: is a prediction of different histologic subtypes possible? *AJNR Am J Neuroradiol* 30(3):591–596. doi:10.3174/ajnr.A1412
8. Kato H, Kanematsu M, Mizuta K, Aoki M (2013) Imaging findings of parapharyngeal space pleomorphic adenoma in comparison with parotid gland pleomorphic adenoma. *Jpn J Radiol* 31(11):724–730. doi:10.1007/s11604-013-0242-4
 9. Minami M, Tanioka H, Oyama K, Itai Y, Eguchi M, Yoshikawa K, Murakami T, Sasaki Y (1993) Warthin tumor of the parotid gland: MR-pathologic correlation. *AJNR Am J Neuroradiol* 14(1):209–214
 10. Ikeda M, Motoori K, Hanazawa T, Nagai Y, Yamamoto S, Ueda T, Funatsu H, Ito H (2004) Warthin tumor of the parotid gland: diagnostic value of MR imaging with histopathologic correlation. *AJNR Am J Neuroradiol* 25(7):1256–1262
 11. Chawla AJ, Tan TY, Tan GJ (2006) Basal cell adenomas of the parotid gland: CT scan features. *Eur J Radiol* 58(2):260–265. doi:10.1016/j.ejrad.2005.12.001
 12. Okahara M, Kiyosue H, Matsumoto S, Hori Y, Tanoue S, Uchida D, Mori H, Kondo Y (2006) Basal cell adenoma of the parotid gland: MR imaging findings with pathologic correlation. *AJNR Am J Neuroradiol* 27(3):700–704
 13. Shi L, Wang YX, Yu C, Zhao F, Kuang PD, Shao GL (2012) CT and ultrasound features of basal cell adenoma of the parotid gland: a report of 22 cases with pathologic correlation. *AJNR Am J Neuroradiol* 33(3):434–438. doi:10.3174/ajnr.A2807
 14. Okahara M, Kiyosue H, Hori Y, Matsumoto A, Mori H, Yokoyama S (2003) Parotid tumors: MR imaging with pathological correlation. *Eur Radiol* 13:L25–L33. doi:10.1007/s00330-003-1999-0
 15. Suh SI, Seol HY, Kim TK, Lee NJ, Kim JH, Kim KA, Woo JS, Lee JH (2005) Acinic cell carcinoma of the head and neck: radiologic–pathologic correlation. *J Comput Assist Tomogr* 29(1):121–126
 16. Kashiwagi N, Takashima S, Tomita Y, Araki Y, Yoshino K, Taniguchi S, Nakanishi K (2009) Salivary duct carcinoma of the parotid gland: clinical and MR features in six patients. *Br J Radiol* 82(982):800–804. doi:10.1259/bjr/29600237
 17. Bewick V, Cheek L, Ball J (2005) Statistics review 14: logistic regression. *Crit Care* 9(1):112–118. doi:10.1186/cc3045
 18. Takeshita T, Tanaka H, Harasawa A, Kaminaga T, Imamura T, Furui S (2004) Benign pleomorphic adenoma with extensive cystic degeneration: unusual MR findings in two cases. *Radiat Med* 22(5):357–361
 19. Layfield LJ, Reznicek M, Lowe M, Bottles K (1992) Spontaneous infarction of a parotid gland pleomorphic adenoma. Report of a case with cytologic and radiographic overlap with a primary salivary gland malignancy. *Acta Cytol* 36(3):381–386
 20. Abiko Y, Kaku T, Shimono M, Noma H, Shigematsu T (1993) Large cyst formation in pleomorphic adenoma. *Bull Tokyo Dent Coll* 34(1):9–14
 21. Nagao K, Matsuzaki O, Saiga H, Sugano I, Shigematsu H, Kaneko T, Katoh T, Kitamura T (1982) Histopathologic studies of basal cell adenoma of the parotid gland. *Cancer* 50(4):736–745